Dalton Transactions

PAPER

Cite this: DOI: 10.1039/c7dt01324h

Oxocomplexes of U(VI) with 8-hydroxyquinoline-5-sulfonate in solution: structural studies and photophysical behaviour†

M. Luísa Ramos, * Licínia L. G. Justino, Rui Barata, Telma Costa, Bernardo A. Nogueira, Rui Fausto and Hugh D. Burrows

Multinuclear (^{1}H and ^{13}C) NMR, and Raman spectroscopy, combined with DFT calculations, provide detailed information on the complexation between U(VI) oxoions and 8-hydroxyquinoline-5-sulfonate (8-HQS) in aqueous solution. Over the concentration region studied, U(VI) oxoions (uranyl ions) form one dominant complex with 8-HQS in water in the pH range 3–6, a mononuclear 1 : 2 (metal : ligand) complex, with the metal centre (UO_2^{2+}) coordinated to two 8-HQS ligands, together with one or more water molecules. An additional minor 1 : 1 complex has also been detected for solutions with a 1 : 1 metal : ligand molar ratio. The geometry of the dominant complex is proposed based on the combination of the NMR and Raman results with DFT calculations. Further information on the electronic structure of the complex has been obtained from UV/visible absorption and luminescence spectra. The complex of U(VI) and 8-HQS is non-luminescent, in contrast to what has been observed with this ligand and many other metal ions. We suggest that this is due to the presence of low-lying ligand-to-metal charge transfer (LMCT) states below the emitting ligand-based and uranyl-based levels which quench their emission. These studies have fundamental importance and are also relevant in the context of environmental studies, and the water soluble ligand 8-HQS has been chosen for application in uranium remediation of aqueous environments.

Received 12th April 2017,
Accepted 8th May 2017

DOI: 10.1039/c7dt01324h

rsc.li/dalton

Introduction

Uranium is the heaviest naturally occurring element in the Earth's crust. Although discovered in 1789, it found few commercial uses for a century and a half beyond its use as a colouring agent for ceramics and glass. Radioactivity was first discovered in uranium in 1896, soon after the discovery of X-rays. Uranium has played a key role in the understanding and exploitation of nuclear energy, both for military and peaceful purposes. Bombarding uranium with neutrons results in lighter elements being formed by nuclear fission, producing large amounts of energy. As ^{235}U, the fissionable isotope, is only 0.71% of natural abundance, whereas ^{238}U is 99.28% of natural uranium, it is necessary to enrich uranium in the ^{235}U isotope for a sustained nuclear reaction. This yields large quantities of uranium that are depleted in fissionable ^{235}U but have a higher percentage of ^{238}U. Developments in ballistics have adopted the depleted uranium as a penetrator in the armament industry.[1] Uranium also has a rich photochemistry,[2] and shows considerable potential in photocatalysis.[3]

Exposure of the general public to uranium is most often by the ingestion of food and water containing natural uranium from the hydrogeological environment. This risk is increased in regions where uranium is mined, milled or processed as well as in the vicinity of earlier battlefields where depleted uranium munitions were installed. The development of incendiary weapons using depleted uranium produced a novel form of uranium environmental contamination, which led to greater exposure to the adverse health effects of the toxic heavy metal after its use in various military conflicts. The aerosol from burning uranium penetrator fragments is rapidly dissolved in biological fluids and readily absorbed by the lungs, leading to a wide range of toxic effects, such as kidney damage and lung cancer.[4] As a consequence, there is increasing interest in the development of stable, water soluble complexes for environmental monitoring and remediation. The coordination chemistry of uranium is also important in areas such as uranium extraction, nuclear fuel reprocessing and treatment of uranium waste.

Centro de Química and Department of Chemistry, University of Coimbra, 3004-535 Coimbra, Portugal. E-mail: mlramos@ci.uc.pt; Fax: +351-239-827703; Tel: +351-239-854453

†Electronic supplementary information (ESI) available. See DOI: 10.1039/c7dt01324h

The aqueous chemistry of its most common oxidation state, uranium(VI), is dominated under acidic conditions by the uranyl ion, $[UO_2(H_2O)_5]^{2+}$, in which the UO_2^{2+} geometry is linear with two oxygen atoms forming multiple covalent bonds to the uranium atom and the five water molecules coordinated in the equatorial plane. The hydrolysis reactions of the uranyl ion, which begin at pH 3, have been the subject of extensive studies, and have recently been discussed in detail.[5] In the presence of chelating ligands, O-, N- and S-donor ligands, the metal ions can form complexes, maintaining the linear $O{=}U{=}O^{2+}$ unit.[6]

The potential impact of hazardous metal ions on the environment has led to the development of novel materials and methods for their detection, quantification, and remediation. Optical sensors, either based on increase in fluorescence or changes in absorption spectra in the presence of metals, are particularly attractive because of their ease of use, high sensitivity, and possibility of incorporating in online detection systems. They can be used over a wide range of analyte concentrations, and applied to real time and space monitoring of these metals.[7,8] Luminescence sensors may emit light of a different wavelength or intensity on binding to a metal from the metal free system. This can provide selectivity, as it depends on the type of metal ion that is bound.[9,10] Free 8-hydroxyquinoline (8-HQ) is only very weakly luminescent, probably because of fast excited state intramolecular proton transfer leading to a nonfluorescent phototautomer.[11] Normally, this pathway is inhibited on complexation, and the dramatic intensity changes seen in the presence of suitable metal ions are the basis for sensitive and selective metal ion sensors.[12] This has been used to develop complex structures with 8-hydroxyquinolates linked to fluorene-based conjugated polymers to enhance sensitivity and selectivity.[7,8] Water soluble 8-hydroxyquinoline derivatives, such as 8-hydroxyquinolone-5-sulfonate (8-HQS), are also good candidates for these applications, and provide a sensitive analytical technique for selective fluorescence detection and quantification of metal ions through steady state[13] or time resolved measurements.[14]

In addition, 8-HQ and 8-HQS also find use as selective sorbents for toxic metals,[15] which are relevant to chelation therapy in patients overcharged with several metals, including uranium metal ions[4,16,17] and are used in optoelectronic devices including organic light emitting diodes (OLEDs). Metal 8-HQS complexes may be incorporated as water-based components into OLEDs through self-assembly in appropriate matrices, such as layered double hydroxides,[18] liquid crystals,[19] surfactants and conjugated polyelectrolytes.[20] Recently, we have carried out a detailed structural and spectral study of the interaction of 8-HQS, with the Zn^{2+} cation and characterized a single 1 : 2 (metal : ligand) complex. This has potential for its fluorescence detection in aqueous media, such as surface waters and biological fluids,[21] and involves a complex with an octahedral geometry having two bidentate 8-HQS ligands and two coordinated water molecules mutually *trans*. With the corresponding 8-HQS complexes of the other group 12 metals Cd^{2+} and Hg^{2+}, again there is a dominant 1 : 2 complex with octahedral coordination. However, the two water molecules here show a *cis* geometry.[22] We have also studied the interaction of 8-HQS with Al^{3+} and Ga^{3+} ions, where three homologous luminescent complexes with 1 : 1, 1 : 2 and 1 : 3 (metal : ligand) stoichiometries were characterized and their geometries were determined.[23,24] These studies were extended to other high oxidation state transition metal ions, and we have characterised 1 : 2 and 2 : 2 (metal : ligand) oxocomplexes of vanadium(V), molybdenum(VI) and tungsten(VI).[25,26] In all cases, luminescence changes were observed in UV-Vis absorption and fluorescence spectra due to metal chelation. This may be used for metal ion detection in an aqueous medium. However, the fluorescence yield was strongly dependent on the nature of the metal ion. On binding to W(VI), 8-HQS shows a marked increase in fluorescence, similar to what has been observed with other metal ions, such as Zn(II) and Al(III). In contrast, with V(V) and Mo(VI), there is only a small change in the 8-HQS fluorescence upon complexation. We suggested that this is due to the presence of low-lying ligand-to-metal charge-transfer (LMCT) states which are close to the emitting ligand-based excited state for V(V) and Mo(VI), and provide an efficient non-radiative pathway for excited state decay. These are at much higher energies for the W(VI) complexes, and this decay route does not occur.

We are interested in extending these studies to other high oxidation state metal ions, and have studied the complexation with U(VI) oxoions. The characterisation of the oxocomplexes formed between U(VI) and 8-HQS, and the determination of their structures are of considerable importance for the above applications.

We report a detailed structural study of the complexation of uranium(VI) metal ions in aqueous solution with 8-hydroxyquinoline-5-sulfonate (8-HQS), using multinuclear NMR (^1H and ^{13}C) and Raman spectroscopy, DFT calculations in parallel with UV/visible absorption and luminescence spectral measurements. Although there have been previous reports on the complexation of U(VI) with 8-HQ and water soluble derivatives, such as 8-HQS,[13,27–29] our knowledge of these systems is far from complete. The equilibrium constants of the 1 : 1 and 1 : 2 complexes have been studied and the 8-HQ and 8-HQS indicated as having potential for use in chelation therapy.[4] However, there is only limited data on the structure of the complexes and, in particular, there is little information on their spectroscopic and photophysical behaviour. While we appreciate that there are likely to be differences in the behaviour of the complexes with this metal ion in solution and in the solid state, for which 1 : 3 metal : ligand complexes have been characterised,[28] we feel that this detailed study of the species present in aqueous solutions is likely to be relevant for applications such as remediation strategies in contaminated soils and in chelation therapy, as an effective chelating agent for control of uranium toxicity. In addition, we believe these results are relevant to understanding how the ligands affect the U=O bonding character.[30]

Experimental section

Materials and solution preparation

Analytical grade uranyl nitrate and commercially available 8-hydroxyquinoline-5-sulfonic acid hydrate were used as received.

For NMR experiments, the solutions were prepared in D_2O and the pH was adjusted by addition of DCl and NaOD; the pH* values quoted are the direct pH-meter readings (room temperature) after standardization with aqueous (H_2O) buffers.

NMR experiments

The ^{1}H and ^{13}C NMR spectra were obtained on a Bruker Advance 500 NMR spectrometer. The ^{13}C spectra were recorded using proton decoupling techniques (Waltz-16) taking advantage of the nuclear Overhauser effect. The methyl signal of *tert*-butyl alcohol was used as the internal reference for ^{1}H (δ 1.3) and ^{13}C (δ 31.2) relative to TMS.

Raman spectroscopy studies

The Raman spectra were obtained in the wavenumber range 100–4000 cm^{-1} for the solid neat ligand and the 1 : 2 uranyl : 8-HQS complex, after evaporation of the solvent (water; pH 5.6), using a Raman micro-system (Horiba LabRam HR Evolution, equipped with a Synapse CCD detector, a high-stability BXFM open space confocal microscope, and a 600 gr mm^{-1} grating) with 633 nm HeNe laser excitation. The laser power at the sample was approximately 17 mW for the 8-HQS spectrum and *ca.* 2 mW for the complex spectrum, and the exposure time was 30 s for both. A 100× objective lens was used, giving a laser spot diameter of 0.8 μm at the sample. Individual spectra were obtained with 1.5 cm^{-1} resolution. The final spectra are the mean of 50 scans for every sample.

UV/visible absorption and luminescence spectral studies

UV/visible absorption and ligand fluorescence, and uranyl luminescence spectra were recorded on Shimadzu UV-2100 and Jobin-Ivon SPEX Fluorolog 3-22 spectrometers, respectively. Fluorescence spectra were registered with excitation at 330 nm (the isosbestic point), and were corrected for the wavelength response of the system. When not being used for measurements, all samples were kept in the absence of light.

Computational details

Density functional theory (DFT) calculations were performed to help determine the structure of the dominant 1 : 2 U(VI) : 8-HQS complex found in water solution. All the molecular structures investigated (closed-shell systems) were optimized at the DFT level of theory employing the B3LYP (Becke three parameter Lee–Yang–Parr)[31,32] exchange correlation functional. The Stuttgart/Dresden[33] small core valence and effective core potential (ECP) functions, adjusted to Wood–Boring quasi-relativistic data, were used for the metal and the standard double-ζ plus polarization 6-31G(d) basis set was used for the expansion of the orbitals of all other atoms. The structures were optimized without any symmetry constraints and considering the bulk solvent (water) effects through the polarizable continuum model (PCM) using the integral equation formalism variant (IEFPCM).[34,35] Calculation of the vibrational frequencies was performed for all the stationary points to make sure that they were true minima (*i.e.*, with no imaginary frequencies). For comparison with the experimental spectra, the Raman spectra were calculated for the structure found for the complex. The calculated vibrational frequencies were scaled by a factor of 0.970 for wavenumbers below 3000 cm^{-1} and 0.953 above that wavenumber. Similarly, for comparison with the UV-Vis spectra, the vertical excitation energies were calculated for the lowest 14 singlet excited states for the complex and the free 8-HQS ligand by time-dependent DFT (TD-DFT) using the CAM-B3LYP[36] functional and the same basis sets used for the ground state calculations. The bulk solvent effects of water were taken into account for the calculation of the Raman frequencies and excitation energies. All the calculations were performed with the GAUSSIAN 09 program.[37]

Results and discussion

NMR studies

Scheme 1 shows the structure of the water soluble 8-hydroxyquinoline-5-sulfonate (8-HQS) ligand.

The proton and carbon chemical shifts as well as the proton–proton coupling constants of 8-HQS have previously been studied in aqueous solution and fully assigned over the whole pH range.[21] The ^{1}H and ^{13}C NMR chemical shifts change with pH, indicating differences in the degree of protonation/deprotonation of the various acidic functions present in the molecule, whilst the proton–proton coupling constants show no significant changes. This indicates that there are no significant conformational changes, such as would be expected for any keto–enol tautomerism.

Clear indications of metal–ligand binding sites can be obtained from broadening or coordination induced shifts of the ^{1}H and ^{13}C signals of the ligand in the presence of the metal ions, compared with those of the free ligand. This, together with metal ion NMR, can provide valuable structural information, including the type of metal centre present in the complexes, as widely exemplified in our previous work on the complexation of metal ions, such as aluminium, gallium and metal oxoions of vanadate, molybdate and tungstate with relevant ligands.[23–26,38–43]

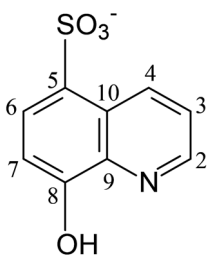

Scheme 1

In addition, with aromatic ligands, inductive effects at specific positions in the aromatic rings allow the identification of changes in the electronic environment together with insights into the nature of the metal–ligand bonds on complexation, and the structure of the chelate species, in particular the symmetry of the coordinated ligands,[44] as illustrated in our studies of the complexation of 8-HQS with Zn^{2+}, Cd^{2+}, Hg^{2+}, Al^{3+}, Ga^{3+}, V(v), Mo(vi) and W(vi).[21–26]

For a complete structural characterization of the interaction of U(vi) ions with 8-HQS, we have obtained ^{1}H and ^{13}C spectra for solutions having 8-HQS concentration of 10 mmol dm^{-3} and U(vi) concentrations ranging from 0 to 10 mmol dm^{-3}, giving metal : ligand molar ratios from 1 : 1 to 1 : 3, and pH* values ranging from 3 to 6. Above pH 6, precipitation occurs.

The results are illustrated in Fig. 1 and 2 for a series of ^{1}H and ^{13}C NMR spectra of 8-HQS alone and in the presence of uranyl nitrate. Two complexes are detected, one dominant, complex **a**, and a minor species, complex **b**, which appear in small concentrations, particularly in solutions with a metal : ligand ratio of 1 : 1.

Distinct signals for the complexed ligands in ^{1}H and ^{13}C NMR spectra are observed, although they appear to be broadened, especially in 1 : 1 solutions, suggesting some exchange on the NMR time scale. NMR studies on certain uranyl chelate complexes have previously indicated some broadening of the peaks associated with ring opening.[45] The ^{1}H and ^{13}C NMR spectral parameters for the system are shown in Tables 1 and 2, respectively.

Species **a** and **b** are detected at pH values between 3 and 6. Species **a** is the only species present in solutions with a 1 : 2 (metal : ligand) molar ratio, while the minor species **b** is observed in 1 : 1 solutions together with species **a**, suggesting that complexes **a** and **b** have 1 : 2 and 1 : 1 (metal to ligand) stoichiometries, respectively. Previous studies have suggested

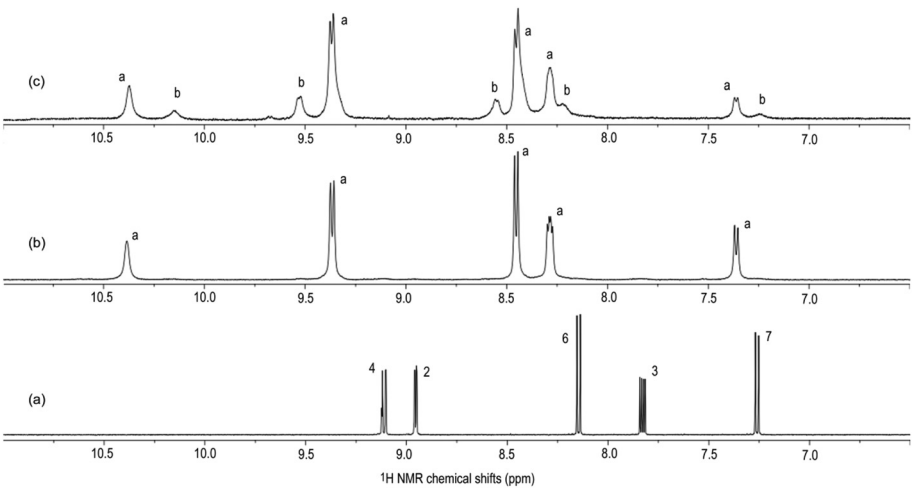

Fig. 1 ^{1}H NMR spectra of D_2O solutions of (a) 8-HQS 10 mmol dm^{-3}, (b) U(vi) : 8-HQS 5 : 10 mmol dm^{-3} and (c) U(vi)/8-HQS 10 : 10 mmol dm^{-3} pH* 5.5, temp. 298 K.

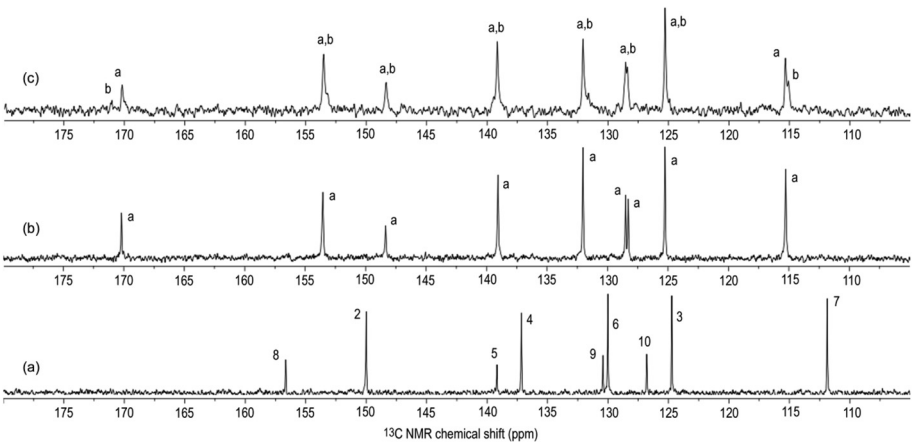

Fig. 2 ^{13}C NMR spectra of D_2O solutions of (a) 8-HQS 10 mmol dm^{-3}, (b) U(vi) : 8-HQS 5 : 10 mmol dm^{-3} pH* 5.5, and (c) U(vi)/8-HQS 10 : 10 mmol dm^{-3}, pH* 5.5, temp. 298 K.

Table 1 ^{1}H NMR parameters[a] for 8-HQS and its complexes with U(VI) (298 K)

	H-2	H-3	H-4	H-6	H-7	$J_{2,3}$	$J_{3,4}$	$J_{2,4}$	$J_{6,7}$
8-HQS[b]									
δ	8.96	7.83	9.11	8.15	7.26	4.4	8.8	1.2	8.2
U(VI) : 8-HQS									
Complex **a**[c]									
δ	10.39	8.29	9.37	8.46	7.37	—	8.6	—	8.2
$\Delta\delta$	1.43	0.46	0.26	0.31	0.11				
Complex **b**[d]									
δ	10.15	8.22	9.55	8.55	7.25	—	—	—	—
$\Delta\delta$	1.19	0.39	0.44	0.40	−0.01				

[a] δ values in ppm relative to Me_4Si using *tert*-butyl alcohol (δ_H = 1.3) as the internal reference; J values in Hz. [b] 10 mmol dm^{-3} 8-HQS solution. [c] 5 : 10 mmol dm^{-3} U(VI)–8-HQS solution. [d] 10 : 10 mmol dm^{-3} U(VI)–8-HQS solution.

the formation of 1 : 1 and 1 : 2 (metal : ligand) complexes between uranium(VI) and 8-HQ, and U(VI) and 8-HQS.[13,27–29]

For complexes **a** and **b**, the nuclei C-2, C-4, C-5, C-6, C-7, C-8, C-9 and C-10 give rise to ^{13}C NMR signals, which undergo significant changes in chemical shifts on complexation, whereas the carbon atom C-3 shows much smaller shifts compared to the free ligand under the same conditions (Table 2). The coordination induced shifts observed for the C-2 and C-8 nuclei support the involvement of deprotonated quinoline (N) and hydroxylate (O) groups in the complexation, as discussed previously.[21,23–26] It is known that the induced shift for a carbon nucleus, which bears a coordinated function results from several contributions to σ_p [46,47] including changes in the electronic density related to the coordination, and to the loss of the O–H proton which occurs upon complexation. Comparing the changes in C-2 and C-8 chemical shifts as a function of pH observed for free 8-HQS with those induced upon metal ion complexation, it can be seen that the chemical shifts of these nuclei parallel the reduced deshielding or shielding observed for C-2 and the large deshielding observed for C-8 upon complexation. C-2 and C-8 nuclei are those most strongly affected by the ionization of the N–H$^+$ (pK_a = 4.09) and C–OH (pK_a = 8.66)[48,49] groups, respectively. The chemical shifts of both C-2 and C-8 nuclei in free 8-HQS increase with pH until around pH 7, while for pH > 7, C-2 chemical shifts decrease as a result of the decreasing of the positive charge of quinoline (N), and C-8 chemical shifts increase with the increasing negative charge of the oxygen atom of the OH group, as we have previously discussed.[21] The observed changes in the other carbon chemical shifts are in agreement with the effects of deprotonation of the ligand upon complex formation.[21,23–26] In particular, the large deshielding observed for C-5 is in accordance with what occurs in this nucleus in the free ligand with increasing pH upon the deprotonation of NH$^+$ and OH.[21] Furthermore, the proton signals are also observed to be shielded or deshielded as a consequence of the deprotonation on complexation, as was observed in previous studies with 8-HQS and 8-HQ, and shown theoretically for pyridine.[44,50]

Considering now the geometrical details, one and two molecules of HQS coordinate the UO_2^{2+} ion in the equatorial plane, in the minor (**b**) and major (**a**) complexes, respectively, with the remaining equatorial positions occupied by coordinated water molecules. The major species, complex **a**, gives rise to one set of ^{1}H and ^{13}C signals, which means that the corresponding nuclei in the two complexed ligand moieties are magnetically equivalent (*i.e.* they have the same ^{1}H and ^{13}C chemical shifts), indicating a symmetrical 1 : 2 complex. This suggests that two molecules of HQS coordinate the UO_2^{2+} ion in the equatorial plane in a symmetrical manner, probably also having one or two water molecules present in the primary coordination sphere.

Raman spectral studies

The 8-hydroxyquinoline-5-sulfonate ligand and the 1 : 2 complex were also investigated by Raman spectroscopy. Fig. 3 presents the Raman spectra of the neat 8-HQS and U(VI)/8-HQS 1 : 2 complex samples. In the spectrum of the complex, bands ascribable to the ligand exhibit significant changes at both positions and intensities compared with the neat ligand, confirming complexation. For example, the intense band at 1377 cm^{-1}, assigned to a mixed C–O stretching/ring stretching vibration, shifts to 1366 cm^{-1}, which is also an indication of the involvement of the oxygen atom of the ligand in the coordination. Deprotonation of the ligand on complexation is confirmed by changes in the OH stretching region (ESI Fig. S1†),

Table 2 ^{13}C NMR parameters[a] for 8-HQS and its complexes with U(VI) (298 K)

	C-2	C-3	C-4	C-5	C-6	C-7	C-8	C-9	C-10
8-HQS[b]									
δ	149.98	124.72	137.15	139.17	130.00	111.87	156.54	130.41	126.79
U(VI) : 8-HQS									
Complex **a**[c]									
δ	153.58	125.29	139.10	148.39	132.07	115.30	170.23	128.54	128.33
$\Delta\delta$	3.6	0.57	1.95	9.22	2.07	3.43	13.59	-1.87	1.54
Complex **b**[d]									
δ	153.07	125.29	139.10	148.39	132.07	115.00	171.01	128.54	128.22
$\Delta\delta$	3.09	0.57	1.95	9.22	2.07	3.13	14.47	−1.87	1.43

[a] δ Values in ppm relative to Me_4Si using *tert*-butyl alcohol (δ_C 31.2) as the internal reference; J values in Hz. [b] 10 mmol dm^{-3} 8-HQS solution. [c] 5 : 10 mmol dm^{-3} U(VI)–8-HQS solution. [d] 10 : 10 mmol dm^{-3} U(VI)–8-HQS solution.

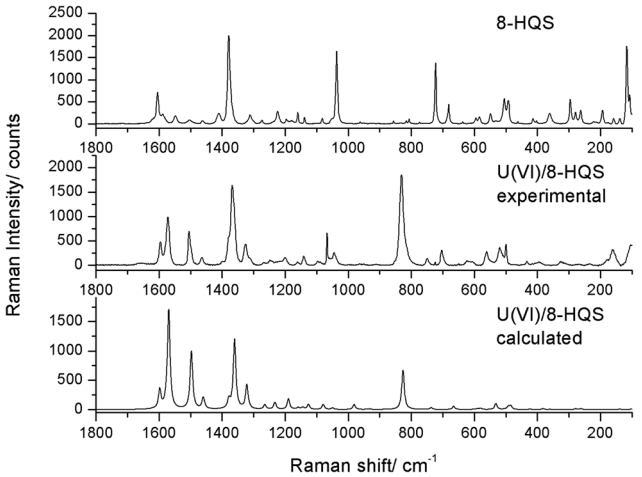

Fig. 3 Raman spectra of 8-HQS (top) and U(VI) : 8-HQS major complex **a** (5 : 10 mmol dm^{-3}; pH = 5.6) (bottom) samples, and the calculated spectrum for the complex (wavenumbers scaled by a factor of 0.970).

where the bands at 3505 and 3398 cm^{-1} in 8-HQS, attributed on the basis of the 8-HQ infrared spectrum[51] to the free and intramolecularly hydrogen bonded O–H group, are absent in the U(VI)/8-HQS complex. Ionization of the ligand is supported by the absence in the spectrum of other bands originating from the OH group of the free ligand at 1410 cm^{-1} (OH in-plane bending) and 722 cm^{-1} (OH out-of-the-plane rocking).

The symmetric and asymmetric stretching bands of the UO_2 group are known to be markedly affected by both the number and nature of ligands bound in the equatorial plane.[52–54] The uranyl ion as its pentaaquo-complex $[UO_2(H_2O)_5]^{2+}$ is known to give rise to bands at 869 cm^{-1} (UO symmetric stretching) and 177 cm^{-1} (bending).[55] In the 1 : 2 complex studied, these bands are observed at 831 and 160 cm^{-1}, respectively. The decrease in the frequency of these uranyl ion modes upon complexation has been reported previously[55–58] and attributed to the overlapping of the non-bonding ϕ_u and δ_u uranium orbitals with the ligand orbitals, leading to a considerable ligand–metal electron density shift. The piling up of charge on the uranium atom then results in the repulsion of the negative oxygen atoms and weakening of the uranium–oxygen bonds. The observed frequency value for the stretching mode is also an indication of the UO_2^{2+} complexation by the ligand in a plane perpendicular to the axial O═U═O direction[55] in complete agreement with the NMR data that the 8-HQS ligands coordinate the uranyl in the equatorial plane.

It is particularly significant that new, moderately intense bands appear at 749 cm^{-1}, ascribable to the O–U–O stretching vibrations (mainly to the more intense symmetric mode) involving the coordinated species. These vibrations are predicted by DFT calculations (see later) to be at *ca.* 735 cm^{-1}. On the other hand, the N–U–N stretching spectral features resulting from the coordination of the 8-HQS ligands through the N atom, predicted by the calculations to occur at *ca.* 665 cm^{-1}, may be ascribed to the band at 702 cm^{-1}.

The calculations also allowed us to propose assignments for other structure-relevant bands observed in the spectrum of the complex: the band at 1463 cm^{-1} has a major contribution from the C–O stretching coordinates of the two ligands (in opposition of phase), the bands at 1161 and 1066/1043 cm^{-1} are due to the stretching modes of the SO_3^- fragment, the first attributed to the anti-symmetric modes and the latter to the symmetric one (these modes are predicted by the calculations at 1143 and 981 cm^{-1}, the latter value being somewhat underestimated); the band at 1141 cm^{-1} is assigned to the C–S stretching modes (calculated frequencies at *ca.* 1126 cm^{-1}); the anti-symmetric O═U═O vibration gives rise to a low intensity band at 913 cm^{-1} (calculated, 930 cm^{-1}); the bands in the 580–480 cm^{-1} spectral region are due to the bending modes of the SO_3^- group; that at 236 cm^{-1} due to the U–OH_2 stretching mode (predicted at 261 cm^{-1}) and the one at 395 cm^{-1} due to the UOC bending modes involving the ligand; the remaining bands exhibiting high to moderate intensity are due to vibrations of the 8-HQS ligand rings, while all the water ligand vibrations not mentioned above are predicted by the calculations to have small Raman intensities and are not observed experimentally (or ascribable to bands of very low intensity with little practical significance).

DFT studies

As indicated in the previous section, the structure of the dominant complex (**a**) has been optimized at the DFT level to help elucidate the coordination mode of UO_2^{2+} with 8-HQS in solution. Since the number of water molecules present in the inner coordination sphere of the major U(VI) : 8-HQS complex formed in aqueous solution is not known, we tried to determine this information using DFT calculations. Several different possible geometries with 0 (two geometries), 1 (two geometries) or 2 (four geometries) coordinated water molecules were optimized. We started by considering the four different geometries with two 8-HQS ligands and two water molecules coordinated in the equatorial plane. These structures have different relative positions of the ligands (*cis* or *trans* positions of H_2O and 8-HQS) and were built taking into account the NMR results, which indicate that the two 8-HQS ligands are magnetically equivalent. The four isomeric structures were optimized, and in all the cases one ligand function was lost (in three of the structures one water ligand was expelled from the inner coordination sphere and in one case one 8-HQS ligand became monodentate). Fig. 4(a) shows this result for the case in which the two water ligands were initially *trans* to each other and the two 8-HQS ligands were symmetrically coordinated relative to a reflexion plane containing the $[O═U═O]^{2+}$ group and the oxygen atoms of the H_2O ligands. In this case, the H_2O molecule coordinated between the two 8-HQS oxygen atoms was expelled from the inner coordination sphere. These findings suggest that a coordination number of 7 is preferred for this U(VI) : 8-HQS complex, with 5 positions occupied in the equatorial plane by two 8-HQS ligands and one water molecule, and the two apical positions occupied by the two terminal oxo ligands.

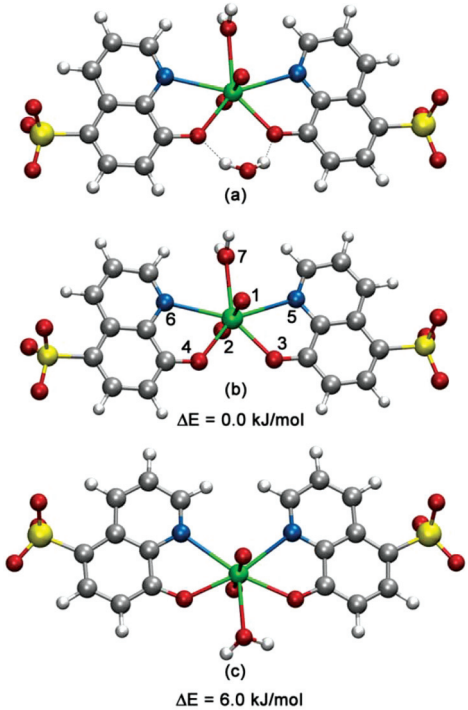

Fig. 4 DFT/B3LYP optimized geometries of (a) $[U(8\text{-}QS)_2(H_2O)_2]^{2-}$ and (b) and (c) the two isomers of $[UO_2(8\text{-}QS)_2H_2O]^{2-}$ (the bulk solvent effects of water were taken into account by using a polarizable continuum model).[34,35]

Table 3 Selected bond lengths (Å) and angles (degrees) calculated with the B3LYP functional for the $[UO_2(8\text{-}QS)_2H_2O]^{2-}$ complex (structure b) taking into account the bulk solvent effects of water[34,35]

	Bond lengths (Å)		Angles (°)
$U–O_1$	1.791	$O_1–U–O_2$	172.59
$U–O_2$	1.791	$O_1–U–O_3$	92.82
$U–O_3$	2.260	$O_1–U–N_5$	89.21
$U–O_4$	2.260	$O_3–U–O_4$	82.27
$U–N_5$	2.690	$N_5–U–N_6$	149.11
$U–N_6$	2.690	$N_5–U–O_7$	74.56
$U–O_7$	2.527	$N_5–U–O_3$	64.31

This type of structure, with one water ligand, allows for two isomers which are compatible with the NMR results. The water molecule can coordinate either between the two N atoms of 8-HQS or between the two hydroxquinolate oxygen atoms. Both structures were optimized and, although caution is needed in interpreting the relatively small energy differences because of factors, such as problems in calculating solvation effects, the first geometry (Fig. 4(b)) appears to be slightly more stable than the second one (calculated ΔG 6.0 kJ mol^{-1}, Fig. 4(c)). Although no symmetry constrains were imposed during optimization, the most stable isomer converged to the C_s point group symmetry. The complex has a distorted pentagonal bipyramidal geometry and the U–N and U–O bond lengths are 2.690 and 2.260 Å, respectively. In the uranyl fragment, the calculated U═O bond length is 1.791 Å and the O═U═O angle is 172.6 degrees (Table 3). These parameters are consistent with those reported in the literature for other U^{VI} complexes,[28,59–63] except for the O═U═O angle, for which the calculated value in this complex is somewhat smaller than those reported in many other uranyl complexes.[64] This is probably caused by the establishment of interactions between the terminal oxo ligands and the water ligand.

UV-Vis absorption and luminescence spectral studies

The addition of uranyl nitrate to an aqueous solution 8-HQS at pH 6 leads to significant changes in the absorption spectra (Fig. 5(a)). Upon addition of the UO_2^{2-} ion, the absorption band at 305 nm (characteristic of 8-HQS species) decreases with the concomitant increase of an absorption at 352 nm. This is close to the absorption maxima seen with other metal ion : 8-HQS complexes, such as $[Zn(8\text{-}QS)_2(H_2O)_2]^{2+}$.[21] The changes in the absorption occur until the UO_2^{2+} : 8HQS molar ratio reaches 0.5 (*i.e.* formation of the 1 : 2 complex). As with the $[Zn(8\text{-}QS)_2(H_2O)_2]^{2+}$ system,[21] the presence of an isosbestic point shows that there is a single equilibrium under these conditions of excess ligand. Above this molar ratio, only minor changes are observed. At the U(VI) concentrations used, the typical weak, structured UO_2^{2+} absorption in the 350–500 nm region[65] was not observed. However, a broad, structureless

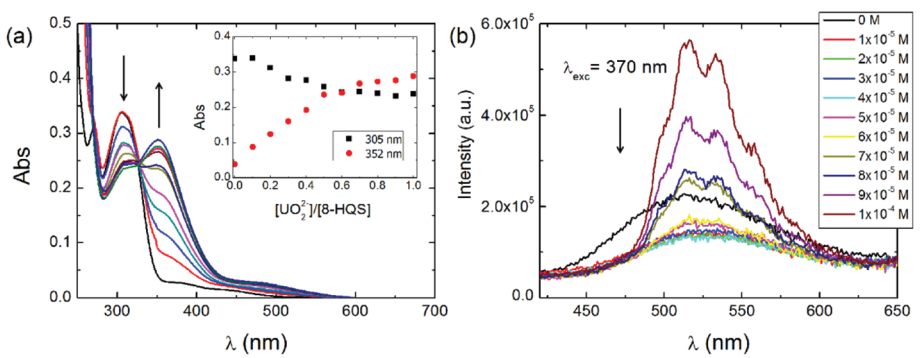

Fig. 5 Absorption (a) and emission (b) (λ_{exc} = 330 nm) spectra of 8-HQS (1×10^{-4} M) in the presence of different concentrations of uranyl nitrate. The arrows indicate the direction of increasing uranyl concentration. Shown as an inset of (a) is the dependence of the absorbance at 305 nm and 352 nm as a function of the UO_2^{2-}/8HQS molar ratio.

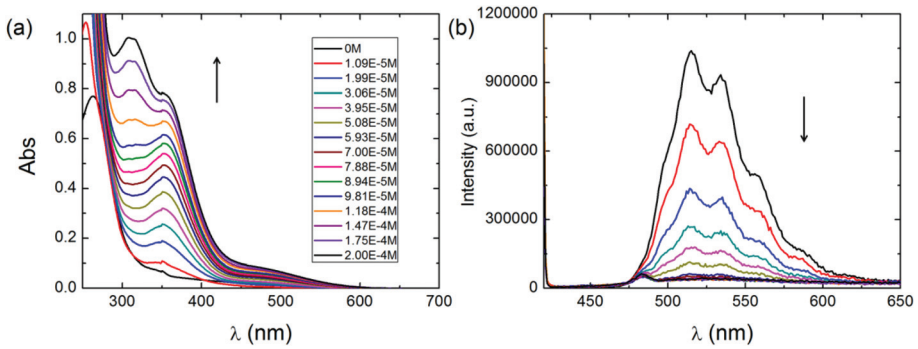

Fig. 6 Absorption (a) and photoluminescence (b) spectra of uranyl nitrate (1×10^{-4} M) in the presence of different concentrations of 8-HQS, λ_{exc} = 415 nm. The arrows indicate the direction of increasing 8-HQS concentration.

band was seen in the 450–600 nm region, which we believe may be associated with a ligand-to-metal charge-transfer transition. The emission spectral behavior upon complexation was studied starting with both pure 8-HQS and pure uranyl ions. The fluorescence spectrum of 8-HQS in the absence and presence of the UO_2^{2-} ion is depicted in Fig. 5(b). In aqueous solution 8-HQS (pH 6) shows a non-resolved emission band with a maximum at 530 nm. This is quenched upon addition of uranyl ions until the molar ratio 0.5 is reached. Above this, the luminescence intensity starts to increase and the characteristic structured emission band of free uranyl ions appears.

We also studied the effect of addition of 8-HQS to an aqueous uranyl nitrate solution at pH 6. In the absence of 8-HQS, we observe the characteristic[65] absorption and emission of the uranyl ions in solution (Fig. 6(a) and (b), respectively). The addition of 8-HQS results in the appearance of the absorption band of the 1 : 2 complex at 352 nm, and in the abrupt quenching of the uranyl emission band, confirming that the added 8-HQS forms a non-luminescent complex with the uranyl ions present in solution. The quenching stops at [8-HQS]/[UO_2^{2+}] = 0.5 (Fig. 7), the vibrational structure of the emission band begins to disappear, and at higher 8-HQS concentrations there is a slight increase of the emission at 530 nm, and the appearance of the absorption band at 305 nm characteristic of free 8-HQS species at pH 6.

Both sets of experiments (Fig. 5–7) indicate the formation of non-emissive UO_2^{2+}/8-QS complexes, with a 1 : 2 stoichiometry. The appearance of a new absorption band at 450–600 nm strongly suggests that the quenching in the fluorescence upon complexation is due to the presence of a low energy ligand-to-metal charge transfer transition.

TD-DFT studies

The electronic structure and bonding in the uranyl ion have been described in detail elsewhere.[66] It has a spin singlet ground state, and emission is from the lowest triplet level. To obtain information on the non-emitting lowest energy excited states, time dependent DFT (TD-DFT) calculations were performed on the $[UO_2(8\text{-QS})_2H_2O]^{2-}$ complex to predict the nature and energies of the 14 lowest singlet excited states. Although the higher excited states do have considerable interest, we restricted ourselves to the low energy region because our particular goal was to confirm the ligand-to-metal charge transfer character of the lowest energy absorption band, and also the higher energy bands in the experimental data are partially masked by absorption from the nitrate ion present in solution. The CAM-B3LYP functional was used to carry out

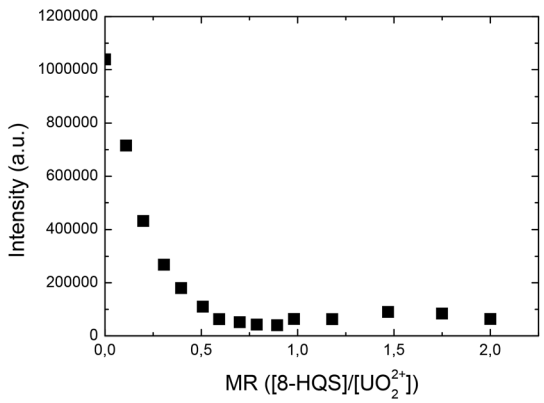

Fig. 7 Fluorescence intensity at the maximum emission wavelength as a function of the [8-HQS]/[UO_2^{2+}] molar ratio.

Table 4 TD-DFT/CAM-B3LYP calculated vertical excitation energies (eV), wavelengths (nm), oscillator strengths and main contributions to the excited state (only the contributions larger than 10% are given) for the $[UO_2(8\text{-QS})_2H_2O]^{2-}$ complex (complex **a**)

	Energy (eV)	λ (nm)	f^a	Main contributions (%)
S_1	2.87	433	0.0005	H → L (82%)
S_4	2.95	420	0.1317	H → L+1 (84%)
S_5	3.06	405	0.0013	H−1→ L (98%)
S_8	3.23	383	0.0028	H−1 → L+1 (100%)
S_9	3.75	331	0.3536	H → L+4 (52%), H−1 → L+5 (48%)
S_{10}	3.75	326	0.0002	H → L+5 (50%), H−1 → L+4 (47%)
S_{14}	4.09	305	0.0134	H−21 → L+1 (62%), H − 25 → L+1 (15%), H → L+1 (12%)

[a] Results are only given for excited states with nonzero oscillator strength.

these calculations since this long-range corrected density functional has been found to give quantitatively accurate results in the investigation of the electronic spectrum of uranyl complexes. In particular, it shows a very significant improvement over B3LYP in the prediction of charge transfer states in these complexes.[67–69] In spite of that, CAM-B3LYP was found to systematically underestimate the local transitions in the uranyl tetrachloride ion $[UO_2Cl_4]^{2-}$, but was capable of predicting the correct ordering of the high-lying states.[68] The vertical excitation energies, oscillator strengths and main transitions contributing to the excited state were calculated at the S_0 optimized geometry and the results are summarized in Table 4. From these results the simulated absorption spectrum of the $[U(8\text{-}QS)_2H_2O]^{2-}$ complex was plotted together with the simulated absorption spectrum of the free ligand 8-HQS (Fig. 8).

The TD-DFT results indicate that the absorption spectrum of $[U(8\text{-}QS)_2H_2O]^{2-}$ has two dominant bands, the stronger one predicted at 331 nm (experimental band at 352 nm) corresponds to a HOMO → LUMO+4 transition (52%) together with a HOMO−1 → LUMO+5 transition (48%), and can be considered to be mainly ligand based with a dominant π → π* character. A second less intense band is predicted at 420 nm and corresponds to the experimental band in the region from 450 to 600 nm. This is essentially a HOMO → LUMO+1 transition (84%). Fig. 9 shows a schematic representation of these transitions and the orbitals involved. The HOMO and HOMO−1 orbitals are localized on the 8-HQS ligands, and to a very small extent on the metal and terminal oxo ligands. The lowest unoccupied orbitals LUMO and LUMO+1 are essentially localized on the metal, whereas the LUMO+4 and LUMO+5 are localized on the 8-HQS ligands. The electronic density distribution in these orbitals tells us that the band calculated at 331 nm is a local excitation localized on the 8-HQS ligand. In contrast, the band calculated at 420 nm is a ligand to metal charge transfer band.

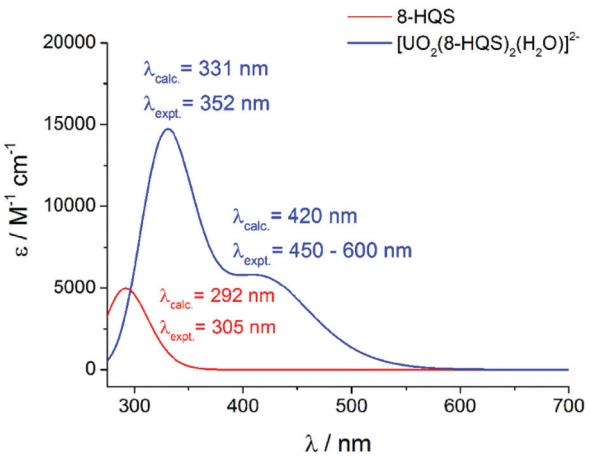

Fig. 8 Simulated TD-DFT/CAM-B3LYP absorption spectra for the free ligand 8-HQS (red line) and the $[UO_2(8\text{-}QS)_2H_2O]^{2-}$ complex (blue line).

Conclusion

The complexation of UO_2^{2+} with the ligand 8-HQS has been studied in aqueous solutions using ^1H and ^{13}C NMR and

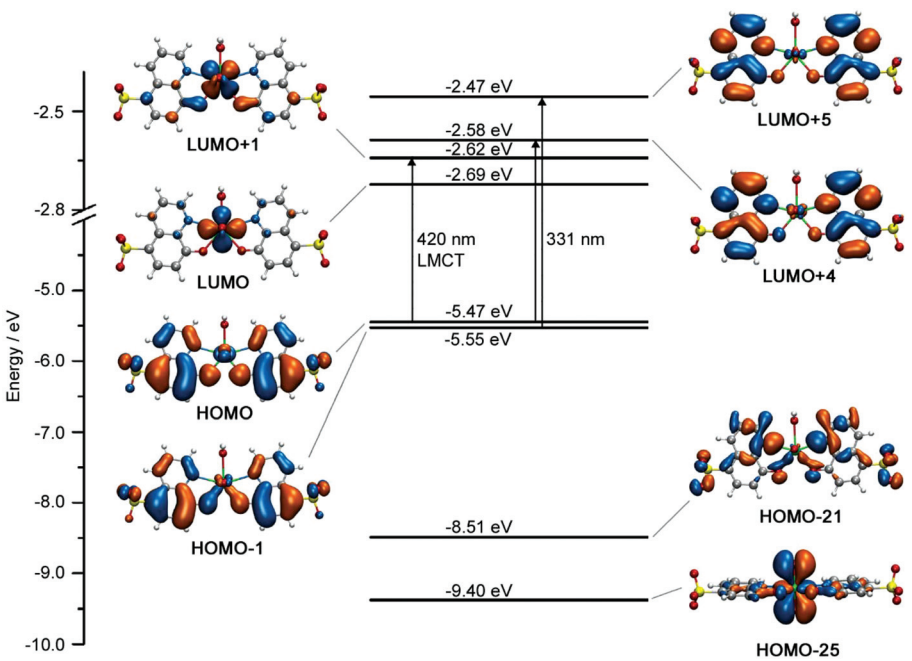

Fig. 9 Orbital density distribution and energies (DFT/B3LYP) for the molecular orbitals involved in the TD-DFT/CAM-B3LYP calculated excitation. Only the transitions involved in the two most intense bands are represented (the orbital density distribution for the orbitals from HOMO−5 to LUMO+5 can be found in ESI Fig. S2†).

Raman spectroscopy and DFT calculations. These indicate a dominant 1 : 2 complex, $[UO_2(8\text{-}QS)_2(H_2O)]^{2-}$, having a distorted pentagonal bipyramidal geometry with a near linear O═U═O group coordinated in the equatorial plane by two chelating 8-hydroxyquinolato-5-sulfonate ligands and one water molecule. This complex has the 8-HQS ligands coordinated in a *cis* geometry, with the lowest energy isomer having the water molecule bound between the two nitrogen atoms of the chelate ligand. At low 8-HQS concentrations, a 1 : 1 complex is formed.

In contrast to many other complexes of 8-HQS with metal ions, and to UO_2^{3+} complexes, the $[UO_2(8\text{-}QS)_2(H_2O)]^{2-}$ complex is not luminescent. UV-Vis absorption and TDDFT calculations indicate this is due to the presence of a lowest energy ligand-to-metal charge transfer state.

Acknowledgements

The authors are grateful for funding from "The Coimbra Chemistry Centre" which is supported by the Fundação para a Ciência e a Tecnologia (FCT), Portuguese Agency for Scientific Research, through the programmes UID/QUI/UI0313/2013 and COMPETE. NMR data were obtained at the UC-NMR facility which is supported in part by the FEDER – European Regional Development Fund through the COMPETE Programme (Operational Programme for Competitiveness) and by the National Funds through FCT with the grants REEQ/481/QUI/2006, RECI/QEQ-QFI/0168/2012, CENTRO-07-CT62-FEDER-002012, and the Rede Nacional de Ressonância Magnética Nuclear (RNRMN). The authors also thank the Laboratory for Advanced Computing at the University of Coimbra for providing computing resources that have contributed to the research results reported within this paper (URL http://www.lca.uc.pt). LLGJ thanks FCT for the postdoctoral grant (SFRH/BPD/97026/2013). BAN is grateful to the Project PTDC/QEQ-MED/3521/2014–POCI01-0145-FEDER-016864 "Photoacoustic Permeabilization of Biological Barriers – A Window for Drug Delivery and Gene Transfection" for the award of a research grant.

References

1 G. D. Lawrence, K. S. Patel and A. Nusbaum, *Pure Appl. Chem.*, 2014, **86**, 1105–1110.
2 L. S. Natrajan, *Coord. Chem. Rev.*, 2012, **256**, 1583–1603.
3 Y. Li, J. Su, E. Mitchell, G. Q. Zhang and J. Li, *Sci. China: Chem.*, 2013, **56**, 1671–1681.
4 A. Š. Joksićab and S. A. Katz, *J. Environ. Sci. Health, Part A: Toxic/Hazard. Subst. Environ. Eng.*, 2015, **50**, 1–10.
5 B. Drobot, R. Steudtner, J. Raff, G. Geipel, V. Brendler and S. Tsushima, *Chem. Sci.*, 2015, **6**, 964–972.
6 D. L. Clark, S. D. Conradson, R. J. Donohoe, D. W. Keogh, D. E. Morris, P. D. Palmer, R. D. Rogers and C. D. Tait, *Inorg. Chem.*, 1999, **38**, 1456–1466.
7 M. A. Palacios, Z. Wang, V. A. Montes, G. V. Zyranov and P. Anzenbacher Jr., *J. Am. Chem. Soc.*, 2008, **130**, 10307–10314.
8 M. A. Palacios, Z. Wang, V. A. Montes, G. V. Zyryanov, B. J. Hausch, K. Jursikova and P. Azenbacher Jr., *Chem. Commun.*, 2007, 3708–3710.
9 A. P. De Silva, H. Q. N. Gunaratne, T. Gunnlaugsson, A. J. M. Huxley, C. P. Mccoy, J. T. Rademacher and T. E. Rice, *Chem. Rev.*, 1997, **97**, 1515–1566.
10 B. Wang and M. R. Wasielewski, *J. Am. Chem. Soc.*, 1997, **119**, 12–21.
11 E. Bardez, I. Devol, B. Larrey and B. Valeur, *J. Phys. Chem. B*, 1997, **101**, 7786–7793.
12 C. H. Chen and J. Shi, *Coord. Chem. Rev.*, 1998, **171**, 161–174.
13 K. Soroka, R. S. Vithanage, D. A. Philips, B. Walker and P. K. Dasgupta, *Anal. Chem.*, 1987, **59**, 629–636.
14 M. Roysen, A. Durandin, V. G. Young Jr., N. E. Geacintov and J. W. Canary, *J. Am. Chem. Soc.*, 2006, **128**, 3854–3855.
15 V. Ravindran, M. R. Stevens, B. N. Badriyha and M. Pirbazari, *AIChE J.*, 1999, **45**, 1135–1146.
16 C. Deraeve, M. Pittié, H. Mazarguil and B. Meunier, *New J. Chem.*, 2007, **31**, 193–195.
17 L. Lannfelt, K. Blennow, H. Zetterberg, S. Batsman, D. Ames, J. Harrison, C. L. Masters, S. Targum, A. I. Bush, R. Murdoch, J. Wilson and C. W. Ritchie, *Lancet Neurol.*, 2008, **7**, 779–786.
18 S. Li, J. Lu, H. Ma, J. Xu, D. Yan, M. Wei, D. G. Evans and X. Duan, *Langmuir*, 2011, **27**, 11501–11507.
19 F. Cameral, J. Barberá, J. Otsuki, T. Tokimoto, Y. Shimazaki, L.-Y. Chen, S.-H. Liu, M.-S. Lin, C.-C. Wu and R. Ziessel, *Adv. Mater.*, 2008, **20**, 3462–3467.
20 H. D. Burrows, T. Costa, M. L. Ramos, A. Valente, B. Stewart, L. L. G. Justino, A. I. A. Almeida, N. L. Catarina, R. Mallavia and M. Knaapila, *Phys. Chem. Chem. Phys.*, 2016, **18**, 16629–16640.
21 M. L. Ramos, L. L. G. Justino, A. Branco, C. M. G. Duarte, P. E. Abreu, S. M. Fonseca and H. D. Burrows, *Dalton Trans.*, 2011, **40**, 11732–11741.
22 M. L. Ramos, L. L. G. Justino, A. Branco, S. M. Fonseca and H. D. Burrows, *Polyhedron*, 2013, **52**, 743–749.
23 M. L. Ramos, L. L. G. Justino, A. I. N. Salvador, A. R. E. de Sousa, P. E. Abreu, S. M. Fonseca and H. D. Burrows, *Dalton Trans.*, 2012, **41**, 12478–12489.
24 M. L. Ramos, L. L. G. Justino, A. R. E. de Sousa, S. M. Fonseca, C. F. G. C. Geraldes and H. D. Burrows, *Dalton Trans.*, 2013, **42**, 3682–3694.
25 M. L. Ramos, L. L. G. Justino, S. M. Fonseca and H. D. Burrows, *New J. Chem.*, 2015, **39**, 1488–1497.
26 M. L. Ramos, L. L. G. Justino, P. E. Abreu, S. M. Fonseca and H. D. Burrows, *Dalton Trans.*, 2015, **44**, 19076–19089.
27 C. F. Richard, R. I. Gustafson and E. Martel, *J. Am. Chem. Soc.*, 1959, **81**, 1033–1040.
28 M. Mirzaei, A. Hassanpoor, A. Bauzá, J. T. Mague and A. Frontera, *Inorg. Chim. Acta*, 2015, **426**, 136–141.
29 J. P. Phillips, *Chem. Rev.*, 1956, **56**, 271–297.

30 S. Tsushima, *Dalton Trans.*, 2011, **40**, 6732–6727.
31 A. D. Becke, *J. Chem. Phys.*, 1993, **98**, 5648–5652.
32 C. Lee, W. Yang and R. G. Parr, *Phys. Rev. B: Condens. Matter Mater. Phys.*, 1988, **37**, 785–789.
33 W. Kuchle, M. Dolg, H. Stoll and H. Preuss, *J. Chem. Phys.*, 1994, **100**, 7535.
34 S. Miertus, E. Scrocco and J. Tomasi, *J. Chem. Phys.*, 1981, **55**, 117–129.
35 J. Tomasi, B. Mennucci and R. Cammi, *Chem. Rev.*, 2005, **105**, 2999–3093.
36 T. Yanai, D. P. Tew and N. C. Handy, *Chem. Phys. Lett.*, 2004, **393**, 51–57.
37 M. J. Frisch, G. W. Trucks, H. B. Schlegel, G. E. Scuseria, M. A. Rob, J. R. Cheeseman, G. Scalmani, V. Barone, B. Mennucci, G. A. Petersson *et al.*, *Gaussian 09, Revision A.02*, Gaussian, Inc., Wallingford, CT, 2009.
38 M. M. Caldeira, M. L. Ramos, A. M. Cavaleiro and V. M. S. Gil, *J. Mol. Struct.*, 1988, **174**, 461–466.
39 L. L. G. Justino, M. L. Ramos, M. M. Caldeira and V. M. S. Gil, *Eur. J. Inorg. Chem.*, 2000, 1617–1621.
40 M. L. Ramos, M. M. Caldeira and V. M. S. Gil, *Carbohydr. Res.*, 1997, **297**, 191–200.
41 M. L. Ramos, M. M. Caldeira and V. M. S. Gil, *Carbohydr. Res.*, 1997, **304**, 97–109.
42 M. L. Ramos, M. M. Pereira, A. M. Beja, M. R. Silva, J. A. Paixão and V. M. S. Gil, *J. Chem. Soc., Dalton Trans.*, 2002, 2126–2131.
43 M. L. Ramos, L. L. G. Justino and H. D. Burrows, *Dalton Trans.*, 2011, **40**, 4374–4383.
44 B. Backer and D. T. Sawyer, *Anal. Chem.*, 1968, **40**, 1945–1951.
45 Z. Szabó, T. Toraishi, V. Vallet and I. Grenthe, *Coord. Chem. Rev.*, 2006, **250**, 784–815.
46 R. K. Harris, *Nuclear Magnetic Resonance Spectroscopy*, Pitman, London, 1983.
47 N. F. Ramsey, *Phys. Rev.*, 1950, **78**, 699–703.
48 J. Fresco and H. Freiser, *Inorg. Chem.*, 1963, **2**, 82–85.
49 T. Le Bahers, C. Adamo and I. Ciofini, *Chem. Phys. Lett.*, 2009, **472**, 30–34.
50 V. M. S. Gil and J. N. Murrell, *Trans. Faraday Soc.*, 1964, **60**, 248–255.
51 G. M. Badger and A. G. Moritz, *J. Chem. Soc.*, 1958, 3437–3442.
52 M. Gál, P. L. Goggin and J. Mink, *J. Mol. Struct.*, 1984, **114**, 459–462.
53 C. Nguyen-Trung, G. M. Begun and D. A. Palmer, *Inorg. Chem.*, 1992, **31**, 5280–5287.
54 G. Lu, T. Z. Forbes and A. J. Haes, *Anal. Chem.*, 2016, **88**, 773–780.
55 L. M. Toth and O. M. Begun, *J. Phys. Chem.*, 1981, **85**, 547–549.
56 S. P. McGlynn, J. K. Smith and W. C. Neely, *J. Chem. Phys.*, 1961, **36**, 105–116.
57 E. Koglin, H. J. Schenk and K. Schwochau, *Spectrochim. Acta, Part A*, 1979, **36**, 641–647.
58 S. Tsushima, *Dalton Trans.*, 2011, **40**, 6732–6737.
59 A. E. Vaughn, D. B. Bassil, C. L. Barnes, S. A. Tucker and P. B. Duval, *J. Am. Chem. Soc.*, 2006, **128**, 10656–10657.
60 H. C. Hardwick, D. S. Royal, M. Helliwell, S. J. Pope, L. Ashton, R. Goodacre and C. A. Sharrad, *Dalton Trans.*, 2011, **40**, 5939–5952.
61 M. Azam, S. I. Al-Resayes, G. Velmurugan, P. Venuvanalingam, J. Wagler and E. Kroke, *Dalton Trans.*, 2015, **44**, 568–577.
62 C. Camp, L. Chatelain, V. Mougel, J. Pecaut and M. Mazzanti, *Inorg. Chem.*, 2015, **54**, 5774–5783.
63 K. Herasymchuk, L. Chiang, C. E. Hayes, M. L. Brown, J. S. Ovens, B. O. Patrick, D. B. Leznoff and T. Storr, *Dalton Trans.*, 2016, **45**, 12576–12586.
64 J. Leciejewicz, N. W. Alcock and T. J. Kemp, *Struct. Bonding*, 1995, **82**, 43–84.
65 H. D. Burrows and T. J. Kemp, *Chem. Soc. Rev.*, 1974, **3**, 139–165.
66 R. G. Denning, *J. Phys. Chem. A*, 2007, **111**, 4125–4143.
67 P. Tecmer, A. S. P. Gomes, U. Ekström and L. Visscher, *Phys. Chem. Chem. Phys.*, 2011, **13**, 6249–6259.
68 P. Tecmer, R. Bast, K. Ruud and L. Visscher, *J. Phys. Chem. A*, 2012, **116**, 7397–7404.
69 P. Tecmer, N. Govind, K. Kowalski, W. A. de Jong and L. Visscher, *J. Chem. Phys.*, 2013, **139**, 034301.